

# Nonmetal-to-metal transition in dense fluid nitrogen at high pressure

Armin Bergermann and Ronald Redmer 

*Institut für Physik, Universität Rostock, D-18051 Rostock, Germany*



(Received 2 May 2023; revised 17 July 2023; accepted 19 July 2023; published 1 August 2023)

We calculate the electrical conductivity and the equation of state of dense fluid nitrogen for high pressures up to several megabars by using *ab initio* molecular dynamics simulations. We determine the instability region of a first-order liquid-liquid phase transition which results from an abrupt dissociation of nitrogen molecules. This transition is accompanied by a nonmetal-to-metal transition (metallization) of the fluid and corresponding structural changes from a molecular to a polymeric phase. We compare our new data with earlier theoretical results and available experiments.

DOI: [10.1103/PhysRevB.108.085101](https://doi.org/10.1103/PhysRevB.108.085101)

## I. INTRODUCTION

The high-pressure phase diagram of *solid* nitrogen is extremely rich: 12 molecular phases, two nonmolecular phases, and an amorphous one have been reported so far [1]. Nitrogen molecules consist of two atoms strongly triple bonded so that corresponding phases can be considered inert. If exposed to high pressure, however, intramolecular bonding becomes weaker, so that double and single bonds also appear. Accordingly, the structural and electronic properties change so that nitrogen passes through several intermediate phases with increasing pressure before covalency is completely lost [2].

Recent molecular dynamics (MD) simulations on dense *fluid* nitrogen using density functional theory (DFT) [3–7] [8,9] predict a first-order liquid-liquid phase transition (LL-PT) at about a megabar. The crossover from a molecular to a polymeric phase is driven by an electronic transition from a molecular semiconducting fluid to a polymeric one with metalliclike conductivity, which has been observed in multiple shock-wave experiments [10].

Excitation, dissociation, and ionization processes are also observed in other shock-compressed diatomic fluids, such as O<sub>2</sub> and CO (which is isoelectronic with N<sub>2</sub>); for a review, see Refs. [2,11]. Most interesting is the metallization in hydrogen (or deuterium) at few megabars [12–15], which, e.g., governs the interior structure, thermal evolution, and dynamo action (magnetic-field generation) of gas giant planets, such as Jupiter and Saturn [16].

In the polymeric phase, each nitrogen atom has single chemical bonds with three surrounding atoms so that this phase could store several times more energy than any known material [2]. This would make polymeric nitrogen an exciting high-energy-density material for corresponding applications.

Numerous high-pressure experiments were performed using diamond anvil cells (DACs) to reveal the high-pressure phase diagram of solid nitrogen and the properties of the different phases; see, e.g., Refs. [2,17,18]. Higher temperatures are generated in shock-wave compression experiments so that dense fluid nitrogen can be probed; see, e.g., Refs. [10, 19–24]. The interesting effect of *shock cooling* due to the dissociation of nitrogen molecules along shock compression

has been predicted by Radousky *et al.* [21] in 1985. The corresponding  $P$ - $T$  conditions are relevant for the interior of ice giant planets, such as Uranus and Neptune. The equation of state (EOS) data in this range are, thus, important for modeling the interior, evolution, and magnetic field of ice giant planets; see, e.g., Refs. [25–32].

Given these important applications, we have reassessed the behavior of dense fluid nitrogen and performed extensive DFT-MD simulations to determine the EOS for temperatures in the range of  $2000\text{ K} \leq T \leq 10\,000\text{ K}$  and densities of  $1.1\text{ g/cm}^3 \leq \rho \leq 4.0\text{ g/cm}^3$ . Analysis of our EOS data shows a systematic shift to higher pressures for given temperatures and densities compared with some earlier studies [3,5]. This trend can be traced back to the use of a higher particle number (256 nitrogen atoms with five electrons each in our calculations versus 64 in Refs. [3,5]), enabled by the enormous progress in computational power over the past decade. The differences are pronounced in the dissociation region so that a new prediction for the instability region of the first-order LL-PT can be given.

We have determined the pair distribution function (PDF) and the coordination number so that the structural changes along the transition can be analyzed as function of density and temperature.

Furthermore, the electrical conductivity was calculated for the entire density-temperature range mentioned above in order to locate the nonmetal-to-metal transition in the  $P$ - $T$ - $\rho$  space. The electrical conductivity increases over about seven orders of magnitude from an almost insulating behavior at the lowest densities and temperatures to values typical for metals at higher densities and temperatures. In these DFT calculations, we have applied the Heyd-Scuseria-Ernzerhof (HSE) hybrid functional [33–36] to determine realistic band gaps, which is essential along the metallization transition. Our results give new insight into the nature of this combined thermodynamic (liquid-liquid, first order) and electronic (metallization) transition in dense fluid nitrogen.

The outline of our paper is as follows. First, we summarize details of the DFT-MD simulations for dense fluid nitrogen in Sec. II. Results for the EOS data are shown in Sec. III, and the structural changes along compression are discussed in Sec. IV

using the pair distribution function. An update of the high-pressure phase diagram is shown in Sec. V. The calculation of the electrical conductivity via the Kubo-Greenwood formula [37,38] is outlined in Sec. VI where we also discuss the nonmetal-to-metal transition in dense fluid nitrogen. Finally, we summarize our results in Sec. VII.

## II. DFT-MD SIMULATIONS

The DFT-MD simulations were performed using the Vienna *Ab initio* simulation package (VASP) [39–43]. The Born-Oppenheimer approximation is used to describe the electron system with DFT at finite temperatures [44–48] and to treat the ions classically via MD simulations. The projector-augmented wave (PAW) potential as implemented in VASP, PAW\_PBE N\_h 06Feb2004, (where PBE represents Perdew, Burke, and Ernzerhof) was used. We used a plane-wave cutoff of 1000 eV, which is considerably higher as in earlier studies. All simulations are performed within the NVT ensemble by using the Nosé-Hoover thermostat [49,50].

We made extensive convergence tests with respect to particle number and chose  $N = 256$  for all DFT-MD simulations for temperatures in the range of  $2000 \text{ K} \leq T \leq 5000 \text{ K}$  and densities of  $2.4 \text{ g/cm}^3 \leq \rho \leq 4.0 \text{ g/cm}^3$ . The first-order LL-PT occurs in this temperature-density range. We found characteristic fluctuations close to the instability region so that large enough particle numbers had to be used. For conditions further away from the LL-PT, our simulations are already converged with  $N = 64$ . The MD simulations were performed with up to 100 000 time steps of 0.6 fs duration, i.e., the chosen NVT ensemble ran up to 60 ps.

We used the exchange-correlation (XC) functional of PBE [51] for all MD runs. Additionally, we employed the HSE hybrid functional [33–36] to evaluate the Kubo-Greenwood formula. The calculation of the electrical conductivity along the nonmetal-to-metal transition required the use of a hybrid functional, such as HSE, which reproduces band gaps and, in particular, their closing with increasing pressure more realistically than PBE; see, e.g., Refs. [52–54].

## III. RESULTS FOR THE EOS

We present the thermal EOS, i.e., the pressure as a function of the density for given temperatures as derived from our DFT-MD simulations in Fig. 1. For clarity, isotherms between  $2000 \text{ K} \leq T \leq 4000 \text{ K}$  are shown in the upper panel, and those between  $4000 \text{ K} \leq T \leq 10\,000 \text{ K}$  in the lower panel, respectively. In accordance with Boates and Bonev [3] and Driver and Militzer [5], we observe an instability region in the dense fluid for lower temperatures, which is highlighted in the inset in the upper panel; see Sec. V.

Our pressures are systematically higher by 10–20% than those of Boates and Bonev [3], which can be attributed to the use of higher particle numbers in our simulations: 256 nitrogen atoms (with five electrons each) compared with 64–128 atoms in their calculations. The higher particle number was necessary to get converged results, particularly, near the dissociation transition. Boates and Bonev [3] used the  $\Gamma$  point, whereas, we used the Baldereschi mean value point (BMVP) [55] to sample the Brillouin zone. Note that Boates

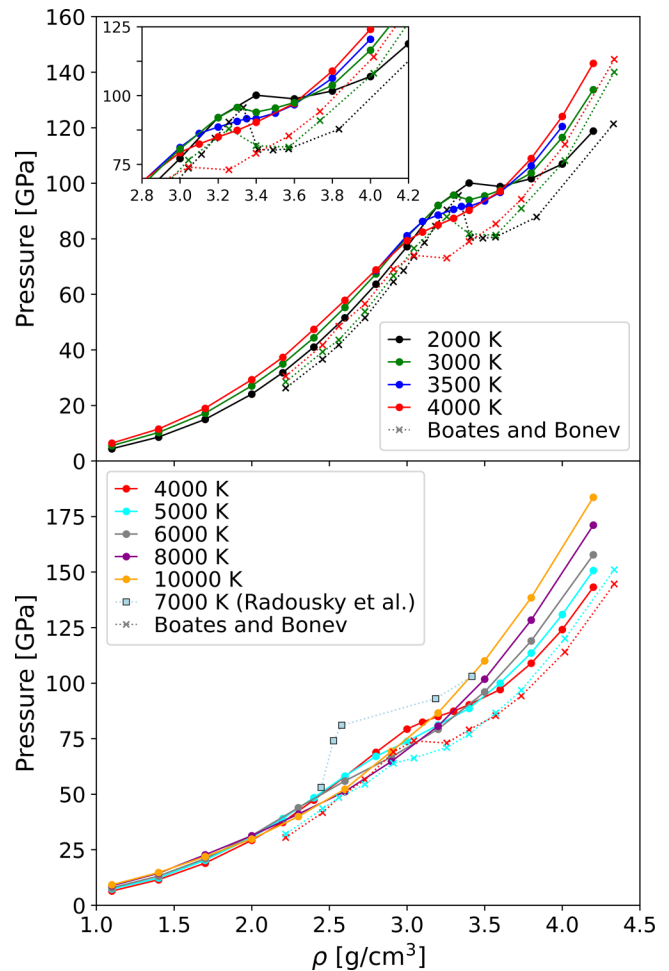


FIG. 1. The pressure of nitrogen is shown as a function of density for temperatures between 2000 and 4000 K (upper panel) and 4000 and 10 000 K (lower panel). We compare our DFT-MD results (solid colored lines with dots) with those of Boates and Bonev [3] (dotted lines with crosses, same color code). Pressures derived from double-shock experiments of Radousky *et al.* [21] are shown as light blue boxes in the lower panel for which a temperature of  $T \approx 7000 \text{ K}$  was reported.

and Bonev [3] predict the stability region above 4000–5000 K, whereas, we derive a critical temperature of  $T_c = 3500 \text{ K}$ , see Sec. V.

In 1985, Radousky *et al.* [21] dynamically compressed fluid nitrogen by using a gas gun. In single-shock experiments, i.e., along the Hugoniot curve, they measured temperatures between  $4000 \text{ K} < T < 14\,000 \text{ K}$  and pressures in the range of  $18 \text{ GPa} < P < 90 \text{ GPa}$ . By performing double-shock experiments, they reported pressures between  $60 \text{ GPa} < P < 90 \text{ GPa}$  at an almost constant temperature of about  $T \approx 7000 \text{ K}$ . The results of these double-shock experiments shown in the lower panel of Fig. 1 as light blue boxes are substantially higher than our results for all temperatures between 4000 and 10 000 K in the density range between 2.4 and  $3.2 \text{ g/cm}^3$ . Radousky *et al.* [21] inferred the temperature by measuring the spectral radiance of the light emitted from the shocked sample. The vast differences between our *ab initio* results and

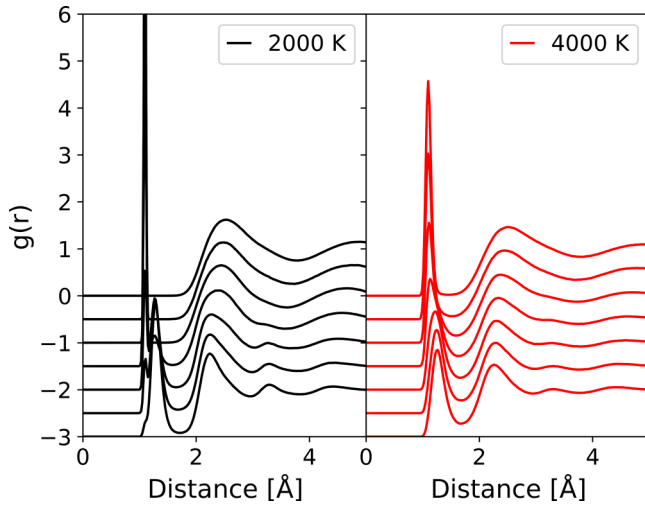


FIG. 2. Pair distribution function in fluid nitrogen for densities of  $\rho = 2.8, 3.0, 3.2, 3.4, 3.6, 3.8,$  and  $4.0 \text{ g/cm}^3$ . The lines are shifted downwards by  $-0.5$  with increasing density. Left panel (black):  $T = 2000 \text{ K}$ , right panel (red):  $T = 4000 \text{ K}$ .

their  $P$ - $T$  data in that density range should be resolved by new shock-compression experiments.

At higher temperatures, the dissociation of nitrogen molecules leads to a reversal of the order of the pressure isotherms above  $1.5 \text{ g/cm}^3$ , see lower panel of Fig. 1. The isotherms return to the usual temperature order only above  $3.5 \text{ g/cm}^3$  in this higher temperature regime. It is interesting to note that the crossing of the isotherms occurs in a much narrower density region for the lower temperatures (upper panel of Fig. 1), i.e., between  $2.7$  and  $3.7 \text{ g/cm}^3$ . The different isotherms clearly show the interplay of thermally and pressure-driven dissociation in dense fluid nitrogen. For higher temperatures, thermally driven dissociation dominates but does not lead to an instability region. In comparison, dissociation occurs more abruptly for lower temperatures, leading to a first-order LL-PT, such as in hydrogen [14,15].

#### IV. RESULTS FOR THE PAIR DISTRIBUTION FUNCTIONS

The PDFs are shown in Figs. 2 and 3, whereas, the coordination number is displayed in Fig. 4. These results can be used to study the structural changes in the fluid as a function of temperature  $T$  and density  $\rho$ .

Figure 2 shows the PDF for  $2000 \text{ K}$  (left panel) and  $4000 \text{ K}$  (right panel) for various densities. For  $2000 \text{ K}$ , a pronounced molecular peak appears at  $1.1 \text{ \AA}$  at lower densities. For densities  $\rho > 3.4 \text{ g/cm}^3$  a second peak at  $1.3 \text{ \AA}$  appears, which can be attributed to the transition from a molecular to a polymeric phase, accompanied by a first-order LL-PT. Several authors have already described this behavior [3–7]. At the higher temperature of  $4000 \text{ K}$ , a shift of the first peak of the PDF from  $1.1$  to  $1.3 \text{ \AA}$  is observed, which proceeds continuously. This shift indicates that the  $CP$  of the first-order LL-PT is located below  $4000 \text{ K}$ , in accordance with the EOS data, see Sec. V. In Fig. 3, the PDF is shown for higher temperatures of  $6000 \text{ K}$  (left panel) and  $10\,000 \text{ K}$  (right panel). Interestingly, the molecular peak at  $1.3 \text{ \AA}$  is still visible even at these

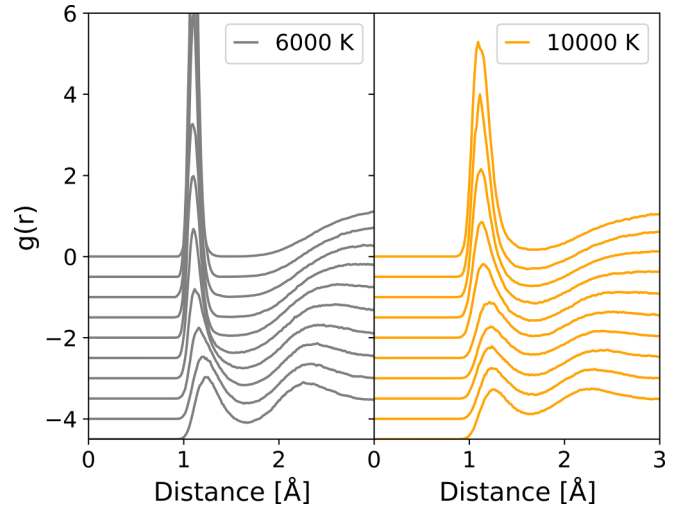


FIG. 3. Pair distribution function in fluid nitrogen for densities of  $\rho = 2.8, 3.0, 3.2, 3.4, 3.6, 3.8,$  and  $4.0 \text{ g/cm}^3$ . The lines are shifted downwards by  $-0.5$  with increasing density. Left panel (gray):  $T = 6000 \text{ K}$ , right panel (orange):  $T = 10\,000 \text{ K}$ .

high temperatures, which indicates that nitrogen transforms gradually to an atomic liquid with increasing density as discussed above.

By integrating the PDF in spherical coordinates up to the first minimum, according to

$$n(r') = 4\pi\rho \int_0^{r'} g(r)r^2 dr, \quad (1)$$

the coordination number is obtained. This quantity indicates how many molecules are found in the range of each coordination sphere by integrating from 0 to the first minimum  $r'$  in the PDF. Therefore, the coordination number signals structural changes in the dense fluid upon compression.

For  $2000 \text{ K}$ , the coordination number is just 1 for densities  $\rho < 3.2 \text{ g/cm}^3$  describing a molecular fluid composed of triple bonded  $\text{N}_2$  molecules. For higher densities, a rapid increase in the coordination number up to 2 and above occurs,

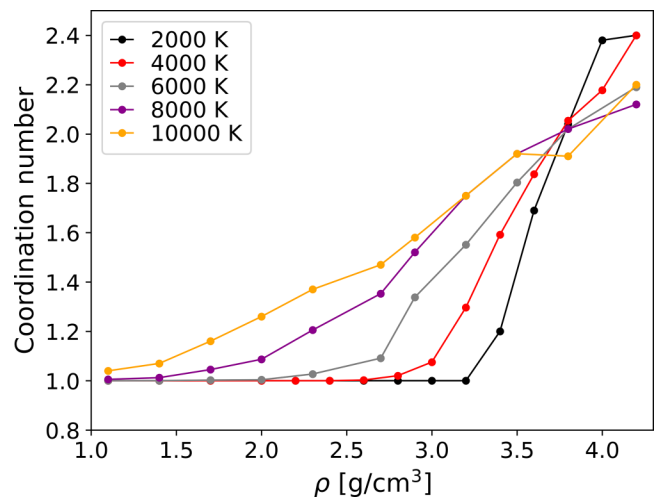


FIG. 4. Coordination number according to Eq. (1) as function of the density for several temperatures:  $T = 2000, 4000, 6000, 8000,$  and  $10\,000 \text{ K}$ .

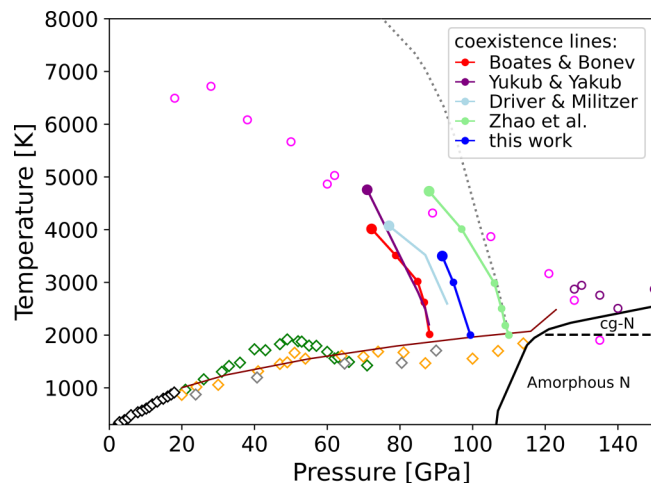


FIG. 5. Phase diagram of nitrogen according to Boates and Bonev [3]. Melting line (diamonds: black [57], green [58], orange [59], gray [60]), polymeric solid phases labeled amorphous and cubic gauche (cgN). The dark-red line represents experimental data for the melting line of Weck *et al.* [61]. Our prediction for the LL-PT (blue line) is compared with that of Boates and Bonev [3] (red line), Yakub and Yakub [56] (purple line), Driver and Militzer [5] (light blue line), and Zhao *et al.* [9] (light green line). Magenta (violet) circles indicate the onset of absorption (reflection) observed in laser-heated DAC experiments [6]. The dotted line represents the phase boundary as predicted by the chemical model of Ross and Rogers [62].

which indicates the transition to the polymeric regime. As seen in the PDF, nitrogen stays molecular even for high temperatures. The increase in the coordination number becomes more gradual with increasing temperature in accordance with the EOS results.

## V. HIGH-PRESSURE PHASE DIAGRAM

The thermodynamic stability condition  $(\partial P/\partial Q)_T \geq 0$  is violated below 3500 K so that a van der Waals loop occurs, which has to be treated by a Maxwell construction. Our numerical results indicate that the critical point for the corresponding LL-PT is located at about  $T_c = 3500$  K,  $\rho_c = 3.4$  g/cm<sup>3</sup>, and  $P_c = 90$  GPa, i.e., the critical temperature is lower than earlier predicted. The coexistence line of the first-order LL-PT is shown as a blue line in Fig. 5, the high-pressure phase diagram adapted from Boates and Bonev [3] with experimental data for the melting line and polymeric solid phases (amorphous and cubic gauche).

According to the EOS data shown in Fig. 1, the coexistence line of the LL-PT is shifted by about 10 GPa towards higher pressures compared with their curve (red line). Yakub and Yakub [56] used the *ab initio* calculations of Boates and Bonev [3] to calibrate an advanced polymerization model. Their prediction for the coexistence line of the LL-PT is shown for comparison (purple line). The prediction of Driver and Militzer [5] for the coexistence line (light blue line) is also based on DFT-MD simulations and located between our result and that of Boates and Bonev [3]. Driver and Militzer [5] have performed their DFT-MD simulations with 64 atoms as Boates and Bonev [3]. The prediction of Zhao *et al.* [9] (green line) is based on DFT-MD simulations using the strongly constrained

TABLE I. Input used in DFT-MD simulations for dense fluid nitrogen. Compared are the XC functional, the number of atoms  $N$ , and the point set for the evaluation of the Brillouin zone (BZ).

Ref.	XC functional	$N$ (atoms)	BZ sampling
Boates and Bonev [3]	PBE	64–128	$\Gamma$
Driver and Militzer [5]	PBE	64	$\Gamma$
Zhao <i>et al.</i> [9]	SCAN	64	$\Gamma$
Fu <i>et al.</i> [7]	PBE	54	$\Gamma$
Mazevet <i>et al.</i> [63]	PW91	32	$\Gamma$
Present paper	PBE and HSE	64–256	BMVP

and appropriately normed (SCAN) meta-generalized gradient approximation functional with 64 atoms. Their LL-PT line lies about 10% above our results in  $P$ - $T$  space. All earlier studies employed the Gamma ( $\Gamma$ ) point to evaluate the Brillouin zone, whereas, we used the BMVP. We summarize the main input into different DFT-MD simulations performed for dense fluid nitrogen in Table I.

Drastic changes in the optical properties of dense fluid nitrogen upon compression were observed in laser-heated DAC experiments. Jiang *et al.* [6] find an onset of absorption (magenta points in Fig. 5) that agrees qualitatively with the continuous transition between the molecular and dissociated fluid above the critical point. The onset of reflection (violet points) indicates the transition to a metallic state at pressures well above a megabar. This transition can be explained by means of the electrical conductivity, which is discussed in the next section.

We also show the prediction of the dissociation model of Ross and Rogers [62] for the molecular-to-polymeric phase transition in the dense fluid (dotted line). They used the experimental data of Refs. [19,21] and calculated the Grüneisen parameter. The corresponding transition pressure is higher than the results of some of the DFT-MD simulations [3,5] including ours but agrees with the SCAN results [9]. The LL-PT line has a different slope for higher temperatures. This behavior is similar to that of the EOS data of Radousky *et al.* [21] shown in the lower panel of Fig. 1. Note that predictions of chemical models have to be treated with caution in the warm dense matter region. The key quantity, the shift in the dissociation energy with density and temperature, is usually treated within simple models which neglect, e.g., effects of disorder (ion structure) and the formation of electronic bands, which are important in this dense fluid regime.

## VI. ELECTRICAL CONDUCTIVITY

The dynamic conductivity  $\sigma(\omega)$  is derived from the Kubo-Greenwood formula, [37,38,64–66],

$$\sigma(\omega) = \frac{2\pi e^2}{3\omega\Omega} \sum_{\mathbf{k}} W(\mathbf{k}) \sum_{j=1}^N \sum_{i=1}^N \sum_{\alpha=1}^3 [F(\epsilon_{i,\mathbf{k}}) - F(\epsilon_{j,\mathbf{k}})] \times |(\Psi_{j,\mathbf{k}}|\vec{v}|\Psi_{i,\mathbf{k}})|^2 \delta(\epsilon_{j,\mathbf{k}} - \epsilon_{i,\mathbf{k}} - \hbar\omega), \quad (2)$$

where  $e$  is the electron charge,  $m$  is its mass,  $\omega$  is the frequency, and  $\Omega$  is the volume of the simulation box.  $\epsilon_{i,k}$  and  $F(\epsilon_{i,k})$  are the energy eigenvalue and Fermi occupation number of the Bloch state  $|\Psi_{i,k}\rangle$  calculated from DFT, and  $\langle \Psi_{j,k} | \hat{v} | \Psi_{i,k} \rangle$  are matrix elements with the velocity operator calculated with the optical routines of VASP [39–43]. The discrete spectrum of eigenvalues is caused by the periodic boundary conditions of the simulation box, so the  $\delta$  function has to be broadened to a finite width for which we use a Gaussian function. Summation over the Brillouin zone is performed by using special  $k$  point sets with weighting factors  $W(\mathbf{k})$ ; for details, see Refs. [66–69].

For temperatures  $T \leq 4000$  K, we evaluated the Kubo-Greenwood formula (2) for 100 snapshots of the MD simulation selected at constant time intervals and used the BMVP to evaluate the Brillouin zone. Performing the simulations with 256 nitrogen atoms, we found the BMVP sufficient to sample the Brillouin zone with the required accuracy. A comparison with Monkhorst-Pack (MP)  $2 \times 2 \times 2$  or  $3 \times 3 \times 3$  point sets revealed no significant differences for our conductivity calculations. This convergence enabled us to calculate the electrical conductivity using the hybrid functional HSE [33–36], which is computationally much more demanding than the PBE XC functional. For higher temperatures  $T > 4000$  K, we used 64 atoms and calculated the conductivity by averaging 20 snapshots. To converge the electrical conductivity at these conditions, we calculated the snapshots with MP  $3^3$  point sets. We used the PBE XC functional for those higher temperatures since the electrical conductivity already has metalliclike values in this range due to the nonmetal-to-metal transition.

The results for the static electrical conductivity are shown in Fig. 6 and compared with those of Boates and Bonev [4]. The calculated densities are the same as given in the EOS, see Fig. 1. In the pressure region between 75 and 100 GPa, we find a substantial increase in the conductivity over several orders of magnitude from values typical for semiconductors up to metal-like conductivities. Below the critical temperature of  $T_c = 3500$  K, the conductivity jumps as a function of pressure from the value of the semiconducting fluid at the low-density branch of the coexistence curve to metal-like values at the high-density branch, which is typical for a first-order phase transition.

Furthermore, we find a strong influence of the XC functional on the conductivity values in the semiconducting fluid. It is well known that the hybrid HSE functional yields more realistic band gaps than PBE [52–54]. The corresponding conductivities are lower by one to two orders of magnitude, dependent on temperature. However, this difference becomes negligible for higher temperatures  $T \geq 6000$  K so that we determined the conductivity solely with PBE in this range. In general, we find a good agreement of our PBE conductivities with those of Boates and Bonev [4].

In 2003, Mazevet *et al.* [63] performed DFT-MD simulations for fluid nitrogen and calculated the conductivity along the Hugoniot curve as well as for the 5000-K isotherm; the latter is shown as cyan diamonds in Fig. 6. They used 32 nitrogen atoms in the simulation cell, the Vanderbilt ultrasoft pseudopotential schema [70], and the Perdew-Wang 91 (PW91)

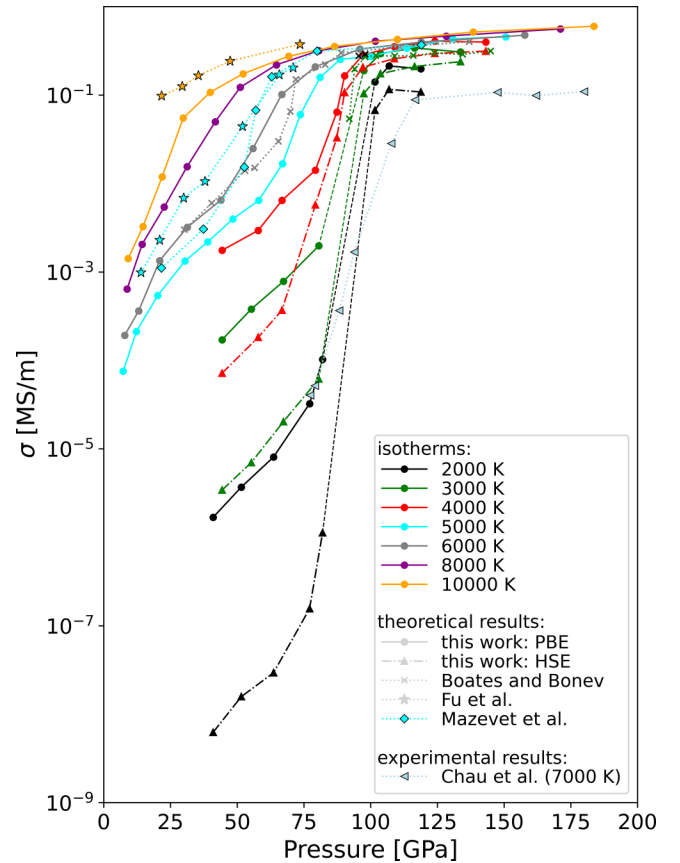


FIG. 6. Static electrical conductivity of dense fluid nitrogen as function of pressure for various temperatures (color coded). PBE functional (this paper): squares, HSE functional (this paper): triangles up. Earlier results based on DFT-MD methods: Boates and Bonev [4]: crosses, Fu *et al.* [7]: stars, and Mazevet *et al.* [63]: diamonds. Experimental data of Chau *et al.* [10] are shown by light-blue triangles left.

parametrization of the generalized gradient approximation [71]. Although we have used more nitrogen atoms in our simulations ( $N = 256$ ) and a different exchange-correlation functional (PBE), we find reasonable agreement. In 2019, Fu *et al.* [7] evaluated the Kubo-Greenwood formula using DFT-MD simulations. They used the PBE functional, the  $\Gamma$  point to sample the Brillouin zone, and 54 nitrogen atoms in the simulation cell. Both studies yield higher conductivities compared to our findings. These deviations can be attributed to higher particle numbers in our simulations and different XC functionals; see Table I.

We also show the conductivities reported by Chau *et al.* [10] derived from double shock-wave experiments using a gas gun in Fig. 6. These data show qualitatively a continuous transition from a semiconducting fluid at lower pressures to a conducting fluid at high pressures, as predicted by the DFT-MD simulations for super critical temperatures  $T \geq T_c$ . Compared to our results, the transition pressure of Chau *et al.* [10] shifts towards higher pressures of  $P \approx 100$  GPa. Furthermore, they assign a temperature of 7000 K to their entire curve, which does not fit at all in the temperature systematics of the DFT-MD simulations. Note that strong doubts have been raised that the treatment of dissociation in the evaluation

of Chau *et al.* is adequate for the dense fluid regime so that their estimate for the dissociation fraction and, consequently, the temperature might be inaccurate [72].

## VII. CONCLUSIONS

We have calculated the EOS data, the structural properties, and the electrical conductivity of dense fluid nitrogen for a wide range of densities and temperatures by using extensive DFT-MD simulations. The enormous increase in computational power enabled us to use significantly higher particle numbers and more advanced XC functionals. We find a first-order LL-PT and locate the corresponding critical point at about  $T_c = 3500$  K,  $\rho_c = 3.4$  g/cm<sup>3</sup>, and  $P_c = 90$  GPa. The electrical conductivity was derived from the Kubo-Greenwood formula using the hybrid HSE functional for temperatures  $T \leq 4000$  K and the PBE functional for higher temperatures. We observe a nonmetal-to-metal transition in the dissociation region with jumps for the electrical conductivity in the instability region as characteristic of a first-order phase transition. The substantially increased computational cost using the hybrid HSE functional pays off since we could determine the electrical conductivity in the semi-conducting molecular fluid at lower temperatures reliably for the first time. The corresponding HSE values are one to two orders of magnitude lower than the predictions of the PBE functional.

Note that the nonmetal-to-metal transition, as observed in dense fluid nitrogen, is very similar to the behavior of

dense fluid hydrogen; see, e.g., Refs. [73,74]. Abrupt dissociation of molecules leads to a first-order LL-PT at lower temperatures. In comparison, the nonmetal-to-metal transition is more gradual at higher temperatures due to additional thermal excitations. The minimum metallic conductivity of  $\sigma_{\min} \approx 2 \times 10^4$  S/m as proposed by Mott [75] originally for liquid mercury and later applied to other materials [76], is exceeded just in the transition region, see Fig. 6.

Our results will promote new experimental campaigns using DACs and/or shock waves to benchmark our predictions for the EOS data and the location of the first-order LL-PT in dense fluid nitrogen. In particular, such experiments will also be performed using DACs and ultrashort and intense x-ray beams provided by free electron laser (FEL) facilities, such as the Linear Coherent Light Source at SLAC Stanford or the European XFEL; see, e.g., Refs. [77,78]. The results presented in this paper underline the importance of new experiments to understand better the behavior of warm dense matter, in general, and of dense fluid nitrogen, in particular.

## ACKNOWLEDGMENTS

We thank M. Preising, M. French, and A. Roy for many helpful discussions and technical support. This work was supported by the North German Supercomputing Alliance (HLRN) and the ITMZ of the University of Rostock as well as by the Deutsche Forschungsgemeinschaft (DFG) via the Research Unit FOR 2440. A.B. thanks the Evangelische Studienwerk e.V. for support.

- 
- [1] R. Turnbull, M. Hanfland, J. Binns, M. Martinez-Canales, M. Frost, M. Marques, R. T. Howie, and E. Gregoryanz, Unusually complex phase of dense nitrogen at extreme conditions, *Nat. Commun.* **9**, 4717 (2018).
  - [2] L. N. Yakub, Polymerization in highly compressed nitrogen (review article), *Low Temp. Phys.* **42**, 1 (2016).
  - [3] B. Boates and S. A. Bonev, First-Order Liquid-Liquid Phase Transition in Compressed Nitrogen, *Phys. Rev. Lett.* **102**, 015701 (2009).
  - [4] B. Boates and S. A. Bonev, Electronic and structural properties of dense liquid and amorphous nitrogen, *Phys. Rev. B* **83**, 174114 (2011).
  - [5] K. P. Driver and B. Militzer, First-principles equation of state calculations of warm dense nitrogen, *Phys. Rev. B* **93**, 064101 (2016).
  - [6] S. Jiang, N. Holtgrewe, S. S. Lobanov, F. Su, M. F. Mahmood, R. S. McWilliams, and A. F. Goncharov, Metallization and molecular dissociation of dense fluid hydrogen, *Nat. Commun.* **9**, 2624 (2018).
  - [7] Z. Fu, Q. Chen, Z. Li, J. Tang, W. Zhang, W. Quan, J. Li, J. Zheng, and Y. Gu, Ab initio study of the structures and transport properties of warm dense nitrogen, *High Energy Density Phys.* **31**, 52 (2019).
  - [8] Y.-S. Lan, Z.-Q. Wang, L. Liu, G.-J. Li, H.-Y. Sun, Z.-J. Fu, Y.-J. Gu, G. Yang, L.-N. Li, Z.-G. Li, Q.-F. Chen, and X.-R. Chen, First-order liquid-liquid phase transition in nitrogen-oxygen mixtures, *Phys. Rev. B* **103**, 144105 (2021).
  - [9] G. Zhao, H. Wang, M. C. Ding, X. G. Zhao, H. Y. Wang, and J. L. Yan, Stability line of liquid molecular nitrogen based on the SCAN meta-GGA density functional, *Phys. Rev. B* **98**, 184205 (2018).
  - [10] R. Chau, A. C. Mitchell, R. W. Minich, and W. J. Nellis, Metallization of Fluid Nitrogen and the Mott Transition in Highly Compressed Low-Z Fluids, *Phys. Rev. Lett.* **90**, 245501 (2003).
  - [11] W. J. Nellis, Dynamic compression of materials: Metallization of fluid hydrogen at high pressures, *Rep. Prog. Phys.* **69**, 1479 (2006).
  - [12] E. Wigner and H. B. Huntington, On the possibility of a metallic modification of hydrogen, *J. Chem. Phys.* **3**, 764 (1935).
  - [13] S. T. Weir, A. C. Mitchell, and W. J. Nellis, Metallization of Fluid Molecular Hydrogen at 140 GPa (1.4 Mbar), *Phys. Rev. Lett.* **76**, 1860 (1996).
  - [14] M. D. Knudson, M. P. Desjarlais, A. Becker, R. W. Lemke, K. R. Cochrane, M. E. Savage, D. E. Bliss, T. R. Mattsson, and R. Redmer, Direct observation of an abrupt insulator-to-metal transition in dense liquid hydrogen, *Science* **348**, 1455 (2015).
  - [15] P. M. Celliers, M. Millot, S. Brygoo, R. S. McWilliams, D. E. Fratanduono, J. R. Rygg, A. F. Goncharov, P. Loubeyre, J. H. Eggert, J. L. Peterson, N. B. Meezan, S. Le Pape, G. W. Collins, R. Jeanloz, and R. J. Hemley, Insulator-metal transition in dense fluid deuterium, *Science* **361**, 677 (2018).
  - [16] R. Helled, G. Mazzola, and R. Redmer, Understanding dense hydrogen at planetary conditions, *Nat. Rev. Phys.* **2**, 562 (2020).

- [17] M. I. Eremets, A. G. Gavriliuk, I. A. Trojan, D. A. Dzivenko, and R. Boehler, Single-bonded cubic form of nitrogen, *Nature Mater.* **3**, 558 (2004).
- [18] P. Cheng, X. Yang, X. Zhang, Y. Wang, S. Jiang, and A. F. Goncharov, Polymorphism of polymeric nitrogen at high pressures, *J. Chem. Phys.* **152**, 244502 (2020).
- [19] W. J. Nellis, H. B. Radousky, C. Hamilton, A. C. Mitchell, N. C. Holmes, K. B. Christianson, and M. van Thiel, Equation-of-state, shock-temperature, and electrical-conductivity data of dense fluid nitrogen in the region of the-dissociative phase transition, *J. Chem. Phys.* **94**, 2244 (1991).
- [20] Y.-J. Kim, B. Militzer, B. Boates, S. Bonev, P. M. Celliers, G. W. Collins, K. P. Driver, D. E. Fratanduono, S. Hamel, R. Jeanloz, J. R. Rygg, D. C. Swift, J. H. Eggert, and M. Millot, Evidence for Dissociation and Ionization in Shock Compressed Nitrogen to 800 GPa, *Phys. Rev. Lett.* **129**, 015701 (2022).
- [21] H. B. Radousky, W. J. Nellis, M. Ross, D. C. Hamilton, and A. C. Mitchell, Molecular Dissociation and Shock-Induced Cooling in Fluid Nitrogen at High Densities and Temperatures, *Phys. Rev. Lett.* **57**, 2419 (1986).
- [22] M. A. Mochalov, M. V. Zhernokletov, R. I. Il'kaev, A. L. Mikhailov, V. E. Fortov, V. K. Gryaznov, I. L. Iosilevskiy, A. B. Mezhevov, A. E. Kovalev, S. I. Kirshanov, Y. A. Grigor'eva, M. G. Novikov, and A. Shuikin, Measurement of density, temperature, and electrical conductivity of a shock-compressed nonideal nitrogen plasma in the megabar pressure range, *J. Exp. Theo. Phys.* **110**, 67 (2010).
- [23] G. L. Schott, M. S. Shaw, and J. D. Johnson, Shocked states from initially liquid oxygen-nitrogen systems, *J. Chem. Phys.* **82**, 4264 (1985).
- [24] W. J. Nellis and A. C. Mitchell, Shock compression of liquid argon, nitrogen, and oxygen to 90 GPa (900 kbar), *J. Chem. Phys.* **73**, 6137 (1980).
- [25] S. Stanley and J. Bloxham, Convective-region geometry as the cause of Uranus' and Neptune's unusual magnetic fields, *Nature (London)* **428**, 151 (2004).
- [26] S. Stanley and J. Bloxham, Numerical dynamo models of Uranus' and Neptune's magnetic fields, *Icarus* **184**, 556 (2006).
- [27] R. Redmer, T. R. Mattsson, N. Nettelmann, and M. French, The phase diagram of water and the magnetic fields of Uranus and Neptune, *Icarus* **211**, 798 (2011).
- [28] N. Nettelmann, R. Helled, J. Fortney, and R. Redmer, New indication for a dichotomy in the interior structure of Uranus and Neptune from the application of modified shape and rotation data, *Planet. Space Sci.* **77**, 143 (2013).
- [29] L. Scheibe, N. Nettelmann, and R. Redmer, Thermal evolution of Uranus and Neptune. I. Adiabatic models, *Astron. Astrophys.* **632**, A70 (2019).
- [30] A. Vazan and R. Helled, Explaining the low luminosity of Uranus: a self-consistent thermal and structural evolution, *Astron. Astrophys.* **633**, A50 (2020).
- [31] L. Scheibe, N. Nettelmann, and R. Redmer, Thermal evolution of Uranus and Neptune. II. Deep thermal boundary layer, *Astron. Astrophys.* **650**, A200 (2021).
- [32] E. Bailey and D. J. Stevenson, Thermodynamically governed interior models of Uranus and Neptune, *Planet. Sci. J.* **2**, 64 (2021).
- [33] J. Heyd, G. E. Scuseria, and M. Ernzerhof, Hybrid functionals based on a screened coulomb potential, *J. Chem. Phys.* **118**, 8207 (2003).
- [34] J. Heyd and G. E. Scuseria, Assessment and validation of a screened coulomb hybrid density functional, *J. Chem. Phys.* **120**, 7274 (2004).
- [35] J. Heyd and G. E. Scuseria, Efficient hybrid density functional calculations in solids: Assessment of the heyd-scuseria-ernzerhof screened coulomb hybrid functional, *J. Chem. Phys.* **121**, 1187 (2004).
- [36] J. Heyd, J. E. Peralta, G. E. Scuseria, and R. L. Martin, Energy band gaps and lattice parameters evaluated with the heyd-scuseria-ernzerhof screened hybrid functional, *J. Chem. Phys.* **123**, 174101 (2005).
- [37] R. Kubo, Statistical-mechanical theory of irreversible processes. I. General theory and simple applications to magnetic and conduction problems, *J. Phys. Soc. Jpn.* **12**, 570 (1957).
- [38] D. A. Greenwood, The Boltzmann equation in the theory of electrical conduction in metals, *Proc. Phys. Soc., London* **71**, 585 (1958).
- [39] G. Kresse and J. Hafner, Ab initio molecular dynamics for liquid metals, *Phys. Rev. B* **47**, 558 (1993).
- [40] G. Kresse and J. Hafner, Ab initio molecular-dynamics simulation of the liquid-metal-amorphous-semiconductor transition in germanium, *Phys. Rev. B* **49**, 14251 (1994).
- [41] G. Kresse and J. Furthmüller, Efficient iterative schemes for ab initio total-energy calculations using a plane-wave basis set, *Phys. Rev. B* **54**, 11169 (1996).
- [42] G. Kresse and J. Furthmüller, Efficiency of ab-initio total energy calculations for metals and semiconductors using a plane-wave basis set, *Comput. Mater. Sci.* **6**, 15 (1996).
- [43] J. Hafner, Ab-initio simulations of materials using VASP: Density-functional theory and beyond, *J. Comput. Chem.* **29**, 2044 (2008).
- [44] P. Hohenberg and W. Kohn, Inhomogeneous electron gas, *Phys. Rev.* **136**, B864 (1964).
- [45] W. Kohn and L. J. Sham, Self-consistent equations including exchange and correlation effects, *Phys. Rev.* **140**, A1133 (1965).
- [46] N. D. Mermin, Thermal properties of the inhomogeneous electron gas, *Phys. Rev.* **137**, A1441 (1965).
- [47] M. Weinert and J. W. Davenport, Fractional occupations and density-functional energies and forces, *Phys. Rev. B* **45**, 13709 (1992).
- [48] R. M. Wentzcovitch, J. L. Martins, and P. B. Allen, Energy versus free-energy conservation in first-principles molecular dynamics, *Phys. Rev. B* **45**, 11372 (1992).
- [49] S. Nosé, Constant temperature molecular dynamics methods, *Prog. Theor. Phys. Suppl.* **103**, 1 (1991).
- [50] W. G. Hoover, Canonical dynamics: Equilibrium phase-space distributions, *Phys. Rev. A* **31**, 1695 (1985).
- [51] J. P. Perdew, K. Burke, and M. Ernzerhof, Generalized Gradient Approximation Made Simple, *Phys. Rev. Lett.* **77**, 3865 (1996).
- [52] M. French, A. Becker, W. Lorenzen, N. Nettelmann, M. Bethkenhagen, J. Wicht, and R. Redmer, *Ab initio* simulations for the material properties along Jupiter's adiabat, *Astrophys. J. Suppl. Ser.* **202**, 5 (2012).
- [53] M. Preising, W. Lorenzen, A. Becker, R. Redmer, M. D. Knudson, and M. P. Desjarlais, Equation of state and optical

- properties of warm dense helium, *Phys. Plasmas* **25**, 012706 (2018).
- [54] M. Guarguaglini, J.-A. Hernandez, T. Okuchi, P. Barroso, A. Benuzzi-Mounaix, M. Bethkenhagen, R. Bolis, E. Brambrink, M. French, Y. Fujimoto, R. Kodama, M. Koenig, F. Lefevre, K. Miyanishi, N. Ozaki, R. Redmer, T. Sano, Y. Umeda, T. Vinci, and A. Ravasio, Multishock comparison of dense gaseous H<sub>2</sub>+He mixtures up to 30 GPa, *Sci. Rep.* **9**, 10155 (2019).
- [55] A. Baldereschi, Mean-value point in the Brillouin zone, *Phys. Rev. B* **7**, 5212 (1973).
- [56] E. S. Yakub and L. N. Yakub, Equation of state and second critical point of highly compressed nitrogen, *Fluid Phase Equilib.* **351**, 43 (2013).
- [57] D. A. Young, C.-S. Zha, R. Boehler, J. Yen, M. Nicol, A. S. Zinn, D. Schiferl, S. Kinkead, R. C. Hanson, and D. A. Pinnick, Diatomic melting curves to very high pressure, *Phys. Rev. B* **35**, 5353 (1987).
- [58] G. D. Mukherjee and R. Boehler, High-Pressure Melting Curve of Nitrogen and the Liquid-Liquid Phase Transition, *Phys. Rev. Lett.* **99**, 225701 (2007).
- [59] A. F. Goncharov, J. C. Crowhurst, V. V. Struzhkin, and R. J. Hemley, Triple Point on the Melting Curve and Polymorphism of Nitrogen at High Pressure, *Phys. Rev. Lett.* **101**, 095502 (2008).
- [60] D. Donadio, L. Spanu, I. Duchemin, F. Gygi, and G. Galli, Ab initio investigation of the melting line of nitrogen at high pressure, *Phys. Rev. B* **82**, 020102(R) (2010).
- [61] G. Weck, F. Datchi, G. Garbarino, S. Ninet, J.-A. Quoyroux, T. Plisson, M. Mezouar, and P. Loubeyre, Melting Curve and Liquid Structure of Nitrogen Probed by X-ray Diffraction to 120 GPa, *Phys. Rev. Lett.* **119**, 235701 (2017).
- [62] M. Ross and F. Rogers, Polymerization, shock cooling, and the high-pressure phase diagram of nitrogen, *Phys. Rev. B* **74**, 024103 (2006).
- [63] S. Mazevet, J. D. Kress, L. A. Collins, and P. Blottiau, Quantum molecular-dynamics study of the electrical and optical properties of shocked liquid nitrogen, *Phys. Rev. B* **67**, 054201 (2003).
- [64] M. French and R. Redmer, Electronic transport in partially ionized water plasmas, *Phys. Plasmas* **24**, 092306 (2017).
- [65] M. Gajdoš, K. Hummer, G. Kresse, J. Furthmüller, and F. Bechstedt, Linear optical properties in the projector-augmented wave methodology, *Phys. Rev. B* **73**, 045112 (2006).
- [66] B. Holst, M. French, and R. Redmer, Electronic transport coefficients from ab initio simulations and application to dense liquid hydrogen, *Phys. Rev. B* **83**, 235120 (2011).
- [67] B. Holst, R. Redmer, and M. P. Desjarlais, Thermophysical properties of warm dense hydrogen using quantum molecular dynamics simulations, *Phys. Rev. B* **77**, 184201 (2008).
- [68] D. Knyazev and P. Levashov, Ab initio calculation of transport and optical properties of aluminum: Influence of simulation parameters, *Comput. Mater. Sci.* **79**, 817 (2013).
- [69] M. French, G. Röpke, M. Schörner, M. Bethkenhagen, M. P. Desjarlais, and R. Redmer, Electronic transport coefficients from density functional theory across the plasma plane, *Phys. Rev. E* **105**, 065204 (2022).
- [70] D. Vanderbilt, Soft self-consistent pseudopotentials in a generalized eigenvalue formalism, *Phys. Rev. B* **41**, 7892 (1990).
- [71] J. P. Perdew, P. Ziesche, and H. Eschrig, *Electronic Structure of Solids '91* (Akademie Verlag, Berlin, 1991).
- [72] M. Bastea, Comment on Metallization of Fluid Nitrogen and the Mott Transition in Highly Compressed Low-Z Fluids, *Phys. Rev. Lett.* **92**, 129601 (2004).
- [73] W. Lorenzen, B. Holst, and R. Redmer, First-order liquid-liquid phase transition in dense hydrogen, *Phys. Rev. B* **82**, 195107 (2010).
- [74] J. M. McMahon, M. A. Morales, C. Pierleoni, and D. M. Ceperley, The properties of hydrogen and helium under extreme conditions, *Rev. Mod. Phys.* **84**, 1607 (2012).
- [75] N. F. Mott, The electrical properties of liquid mercury, *Philos. Mag.* **13**, 989 (1966).
- [76] P. P. Edwards, M. T. J. Lodge, F. Hensel, and R. Redmer, '... a metal conducts and a non-metal doesn't', *Phil. Trans. R. Soc., A* **368**, 941 (2010).
- [77] U. Zastra, The high energy density scientific instrument at the European XFEL, *J. Synchrotron. Rad.* **28**, 1393 (2021).
- [78] R. Husband, A MHz X-ray diffraction set-up for dynamic compression experiments in the diamond anvil cell, *J. Synchrotron Rad.* **30**, 671 (2023).